applied sciences

MDPI

Article

Primary Seal Deformation in Multipane Glazing Units

Bojan Starman [1], Andraž Maček [1], Primož Rus [1], Štefan Obid [1], Aleš Kralj [2] and Miroslav Halilovič [1,*]

[1] Faculty of Mechanical Engineering, University of Ljubljana, Aškerčeva 6, 1000 Ljubljana, Slovenia; bojan.starman@fs.uni-lj.si (B.S.); andraz.macek@fs.uni-lj.si (A.M.); primoz.rus@fs.uni-lj.si (P.R.); stefan.obid@fs.uni-lj.si (Š.O.)

[2] Reflex Gornja Radgona d.o.o., Podgrad 4, 9250 Gornja Radgona, Slovenia; ales.kralj@reflex.si

* Correspondence: miroslav.halilovic@fs.uni-lj.si

Received: 19 January 2020; Accepted: 14 February 2020; Published: 19 February 2020

Featured Application: The presented topic is related to the development of a new six-pane facade glazing unit Q-Air that has been recently successfully put on the market (http://www.reflex.si/en/q-air). During R&D, the herein presented methodology for the durability assessment has been developed based on theoretical mechanics principles and used as a tool in a design phase for different types and sizes of glazing units.

Abstract: Quadruple glazing has become a high-end standard in the field of sealed insulating glass units. With more than three glass panes a set of internal heat-related technical problems emerges. Durability, being the most pressing problem, requires careful management of the primary sealant deformation, especially under summer environmental conditions. Namely, the role of the primary seal in insulating glass units is to protect their humidity-sensitive, low-emissivity coatings from moisture and the quality of such protection is a key factor in durability. In this paper, a new methodology is proposed for a feasibility assessment of a new multipane insulating glass unit design, where proper design enables avoidance of excessive strain on the primary seal. It focuses on the calculation of the primary sealant strains, which are nonhomogeneous and multiaxial according to different loading conditions. This approach leads to analytical expressions that enable convenient identification of the critical location on the primary sealant. Finally, feasibility is assessed with the proposed methodology for the newly developed highly insulative six-pane facade unit by means of a comparison of the calculated strain state with the anticipated allowable strains, based on technical practice.

Keywords: edge-seal failure; durability; strain state; quadruple glazing; multipane glazing

1. Introduction

In 1865, Stetson patented the first double glass unit (DGU) as an improvement of window glass that effectively reduces heat loss and improves sound protection [1]. The first insulating glass unit (IGU) was single-sealed and was soon improved by a desiccant in order to protect the interior side of the glass panes from condensation. In the late 1970s, edge seal design was improved in order to increase durability. Double-sealed IGUs were introduced, which have a primary seal between the spacers and glass, and a secondary seal above the spacers. The primary sealant is usually polyisobutylene (PIB) and, due to its thermoplastic mechanical behaviour, it can be described as a non-structural component. Its main role is to protect the insulating chambers against water vapour permeation. The secondary sealants, i.e., polysulphides, polyurethanes, or silicones [2,3], represent a mechanical restraint that

holds the primary seal in place and defines the structural integrity of the IGU. The importance of sealant systems in IGUs is thoroughly elaborated in [4].

1.1. Issues and Limitations of IGU Durability

The major limitation regarding the service life of an IGU is vapour condensation fogging in the insulating chambers, i.e., on the internal glass surfaces. The durability of units is therefore related to the water vapour permeability of the edge seal, which was experimentally examined in [5], where time to fogging was predicted based on measurements of the dew point temperature of the cavity gas fill in IGUs under several ambient conditions. The moisture content in the insulating chambers was experimentally examined in [6] and can be assessed using standards for IGU durability testing [7]. A novel experimental method for diffusion gas loss in IGUs was presented in [8].

Multipane glazing units are attractive due to high energy efficiency of those buildings where they are built-in [9]. However, in multipane glazing arrangements (i.e., in glazing with more than three glass panes) a further restriction stems from the maximum permitted operating temperature of the PIB primary sealant. In two-pane and three-pane arrangements an 80 °C temperature limit [10] is difficult to exceed; however, exceeding the maximum permitted PIB temperature is easy in multipane arrangements [10].

The water vapour permeability of the dual-edge seal is almost exclusively determined by the permeability of the primary sealant because the permeability of the secondary sealant is significantly lower [11]. However, the diffusion process, as a main component of the gas permeability in the primary sealant, is exponentially dependent on temperature [12], hence resistance to atmospheric loads is the lowest during the summer. Not only a change in the material properties, but also the deformation caused by climatic loads plays a crucial role in the longevity of any IGU. Increased temperature causes a pressure increase in the insulating chambers. The pressure deflects the glass panes and the consequent change in the pressure and chamber volume is dictated by the ideal gas law. Thin glass panes enable a higher chamber volume change due to lower stiffness, which compensates for the pressure increase and lowers the pressure load on the edge seal. However, high edge seal displacements are not acceptable from a durability point of view and also due to the potential risk of glass failure [13]. Therefore, glass panes normally feature significant stiffness, which results in a pressure increase in the insulating chambers that further stretches the edge seal. Such stretching has a direct influence on moisture permeation because the deformed effective diffusion cross-section of the primary seal increases and the diffusion length decreases.

A double-seal system between two glass panes is made of two layers perpendicular to the glass: in the first one there is a spacer and a primary sealant, and the second layer enveloping the first layer represents a secondary seal. From a mechanical point of view, there are two parallel elements subjected to the same displacement, but the strains in the two sealants differ significantly. While the strain in the secondary seal is nearly homogeneous, the primary seal has to compensate for the vast majority of the displacement due to the underlying spacer stiffness. The described phenomenon is experimentally well documented together with the development of a new type of spacer in [14] and confirmed by measurements of the gas concentration decrease in the IGU's insulating chamber [15]. Therefore, in a typical IGU, the strain on the primary sealant is significantly higher than the corresponding strain on the secondary sealant.

Furthermore, the material properties of both sealants also differ significantly. The primary sealant is a thermoplastic-like liquid and is not employed as a structural component. It stretches and compresses as it is forced by the surrounding structural components. As long as the elastic deformation remains small, cyclic straining is mainly reversible. Under cyclic loading, a pumping action is observed [16] and the excessive opening between the spacer and the glass can overstretch the primary sealant.

The role of the secondary sealant, which is a structural elastomeric material, is to restrain the extension of the edge seal because the extension of the secondary seal determines how much the primary

seal is permitted to deform under the expected load. As a matter of concept, once the load is reduced again, elastic recovery of the secondary sealant forces the primary sealant into its original position.

The elastic recovery of the secondary sealant is temperature-dependent and if it is not able to recover, the primary seal remains permanently deformed until negative pressure compresses the primary seal [11]. The described phenomenon increases the effective cross-section for the diffusion of moisture. Both seals are also water-sensitive and must be protected from both rain and condensed water. Any secondary seal swelling directly affects the primary seal stretching and must be avoided [17].

1.2. State of the Art

It has been recognised that IGU durability is mainly dependent on the primary seal [18], hence this aspect has been extensively investigated [19]. A thorough state-of-the-art review of a large number of primary seal systems and comparison of the performance thereof is presented by Bergh et al. [2]. Song et al. [20,21] addressed the influence of spacer material on the inside surface condensation. In [22] Wolf describes the impact of the spacer rigidity and thermal expansion coefficient (CTE) on the PIB seal deformation under various loadings. It was found that a stainless-steel spacer had less effect on the change in the PIB cross-section due to the lower CTE, while an aluminium spacer had the largest effect due to the high CTE. In order to homogenise the strain in the primary sealant, a new warm edge system, i.e., Ködispace, was developed [14]. In such a double glass unit (DGU) there is a primary seal only between two glass panes, while in multipane glazing there are more interacting systems, which significantly complicates IGU design.

Recently, multipane IGUs have appeared on the market; Grynning et al. analysed and compared their performance in [23]. The authors exposed pressing issues that are specific to multipane IGUs. Namely, in multipane glazing the intermediate chambers are highly insulated by the other chambers, therefore high cavity temperatures due to solar energy absorption can pose a problem for the robustness of such units. There are several layers of PIB and their mechanical behaviour can differ significantly from one layer to another and also along the circumference. The design requirements for such a complex structure were partially disclosed in [10].

A numerical approach is one of the possibilities to gain insight into the mechanical behaviour of an IGU. Hagl [24] performed compressive tests of edge seal spacers and built a numerical model for the sake of comparison. Stewart et al. [25] used the finite element method (FEM) to analyse the thermal displacements of the spacer frame and glass panes. However, to obtain the PIB response, the entire IGU should be exactly modelled, which requires very dense mesh and expensive analyses.

1.3. Study Aims

A determination of the strain field of all PIB layers seems an almost impossible task for several reasons. The most obvious is the PIB mechanical and rheological nonlinearity, which results in loading history-dependent behaviour. Even if a specific cyclic loading over the lifetime of the unit were somehow known, there are too many geometrical and material uncertainties that make a calculation of the exact PIB shape over several years highly unreliable. In order to obtain some guidelines for multipane IGU design, a comparative approach to assessing PIB longevity is undertaken herein.

From the IGU durability point of view, the longevity of the primary sealant is one of the major concerns. Based on the assumption that primary sealant longevity is closely related to primary sealant deformation, this paper deals with primary seal strain under different loading conditions. There is no intention herein to derive the primary sealant strain state after years of loading, but to develop an alternative methodology that provides a feasibility assessment for any new IGU design.

The methodology is based on the idea that primary sealant strains can be classified according to type of strain (normal, shear) and the intensity thereof. The type of strain can be obtained by analysing each loading case, i.e., the bulging of the IGU due to temperature increase in the chambers, temperature expansion of IGU components, dead weight, wind, etc. Each deformation mode of the seal, presented in Section 2, and the combined effect of their influences are analysed, as presented in Section 3. The most

important theoretical contribution of the paper is given in Section 4, where analytical expressions for primary seal strains are derived for the most significant deformation mode. Once the strains are classified, the intensity needs to be assessed. Since there exist no allowable values in this regard, they have to be determined from technical practice. Here we rely on the fact that there already exist older IGUs that have been on the market for a long time and their durability has been proven through real application in civil engineering. Analysing such older IGUs by the methodology presented in Section 5.1 gives allowable strains for the new IGU, which is analysed using the same methodology in Section 5.2. Here it is assumed that if the primary sealant withstood a certain level of strain of a specific type in the older IGU, then the primary sealant in the new IGU is capable of withstanding the same strain level. The presented methodology has been implemented in the development of a new six-pane glass unit Q-Air, which has been successfully put on the market, as briefly presented in Section 5.3.

The main aim of this work is herein presented derivation of analytical strain field calculation, which represents a shortcut in order to avoid time-consuming FEM analyses of primary sealant behaviour, thus final analytical equations serve as a useful tool in a design phase for fast calculations and feasibility assessment of each particular panel configuration. A feasibility of assumptions used in derivation is confirmed by comparison of analytical and FEM results.

2. Methodology

Since there are no general criteria regarding the sealant system strain-stress state for determining the serviceable IGU lifetime, it can be deduced from the abovementioned literature where PIB strain is the limiting factor. The strain state is not equal in all PIB layers and varies along the circumference of the IGU as well. It is reasonable to assume that the location of maximal strain with proportional loading from the initial state represents a critical point also for cyclic loading and thus is the decisive factor in high-performance IGU lifespan.

Figure 1 shows a schematic representation of different strain modes that occur under loading conditions in a single-chamber double-glass unit (DGU). The climatic conditions, including solar radiation, influence the temperature of the glass panes and gas within the chamber. The glass panes' dimensions vary vs. the spacer due to temperature change, and the elongation differences between the panes and spacer cause shear strains, as presented by modes A and B of the elementary PIB volume. The heat-related pressure increase in the chamber generates the extension of the PIB, shown as mode D. Furthermore, the edge rotates due to the consequent glass pane bulging, which causes shear and normal strain on the inner and outer sides of the PIB, shown as mode C.

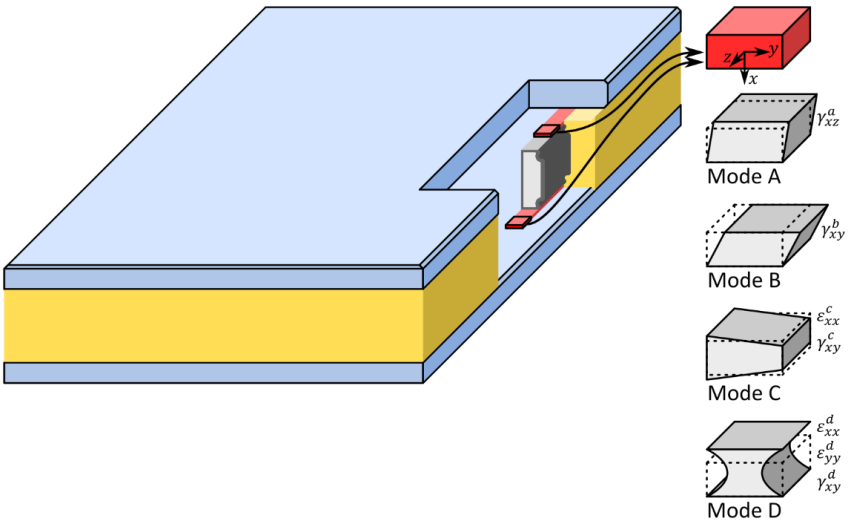

Figure 1. Polyisobutylene (PIB) deformation modes.

To summarize, in the PIB there is a complex strain state with the non-zero strain components being γ_{xz}, γ_{xy}, ε_{xx}, and ε_{yy}. It should be noted that strains due to other loading types, such as self-weight or wind-load, are of the same type and can be algebraically added to these strains. In order to estimate the critical strain state, the following approach is proposed:

1. First, we determine the assumed quasi-steady-state temperature field of the analysed IGU structure. According to the prescribed climatic conditions (including solar radiation-induced internal heating), individual pane temperatures are determined. With all glass-pane temperatures known, the temperatures of other structural elements may be determined using linear interpolation, which is an approximation of the alternative 3D heat transfer analysis. The temperature field serves as the input data for the subsequent thermo-mechanical analysis.
2. A 3D finite element method (FEM) thermo-mechanical IGU model is built, where the mechanical influence of the PIB on the global mechanical response of the structure is neglected. Although the same assumption was also applied by Stewart et al. in [25], PIB notably contributes to the rigidity of the seal system when cold. However, due to the exponential growth of vapour permeation with increasing temperature, the primary longevity-related issue is the summer, when the PIB is also soft and its mechanical rigidity really becomes negligible. Additional mechanical loads, e.g., wind load and self-weight, can be optionally added. The analyses give a reliable strain-stress state for all structural components, except for the omitted PIB. However, the results include the displacements of the glass panes and spacers to which the PIB is attached. These displacements are the input data for the identification of the type and severity of the PIB deformation modes, as presented in Figure 1.
3. The extracted, numerically determined, displacements represent the boundary conditions for the shear and normal strain calculations of the PIB for all deformation modes separately.
4. In accordance with the superposition principle, the analytically calculated strains for all deformation modes are summed into a strain tensor for each point of the PIB along the unit's circumference and for all PIB layers. Lastly, an equivalent strain calculation serves for the final comparative evaluation.

Each step will be described in detail in the next section, where the approach is applied to a six-pane Q-Air glazing unit [10] with a specific large-unit design, 10-18-4-18-4-18-4-18-4-18-66.4, cf. Figure 2. This consists of 10 PIB layers designed to be 0.3 mm thick. Their precise inclusion in the full 3D FEM model would be too taxing due to the extremely fine mesh required to adequately model the strain field [26].

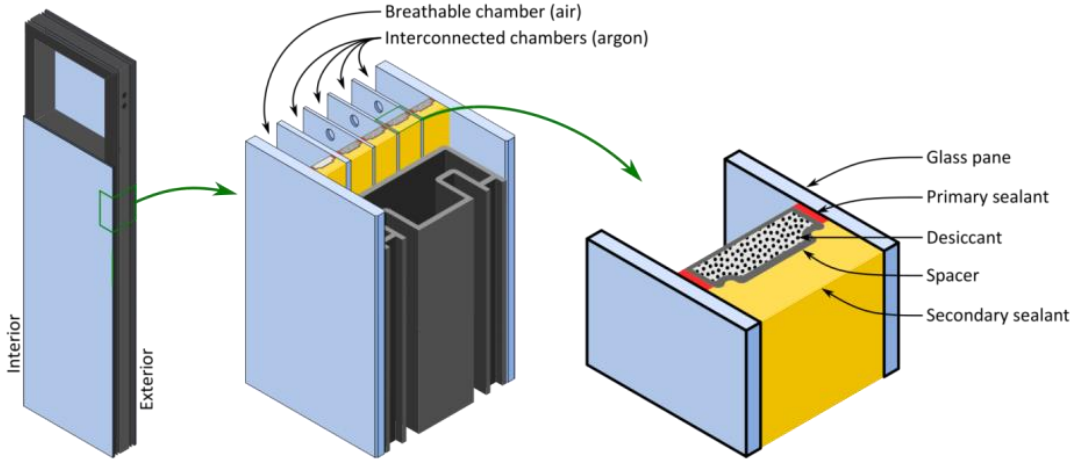

Figure 2. Six-pane Q-Air glazing unit.

3. Numerical and Analytical Calculations

3.1. Individual Pane Temperature Calculations

Pane temperatures for the six-pane IGU are calculated using LBNL (Lawrence Berkeley National Laboratory) Window 7.4 software [27]. Glass pane temperatures for 90% argon-filled sealed glass blocks with 18 mm spacers are calculated under the following climatic conditions: 40 °C exterior temperature, stagnant air, 24 °C interior temperature, and 783 W/m^2 solar radiation. The method was experimentally verified in [10].

The temperatures of the other components were estimated using linear interpolation, as shown in Figure 3. The gas temperature in each individual cavity is set to the average of both neighbouring glass panes. The temperature field of the unit is used as the input data for the subsequent mechanical analysis.

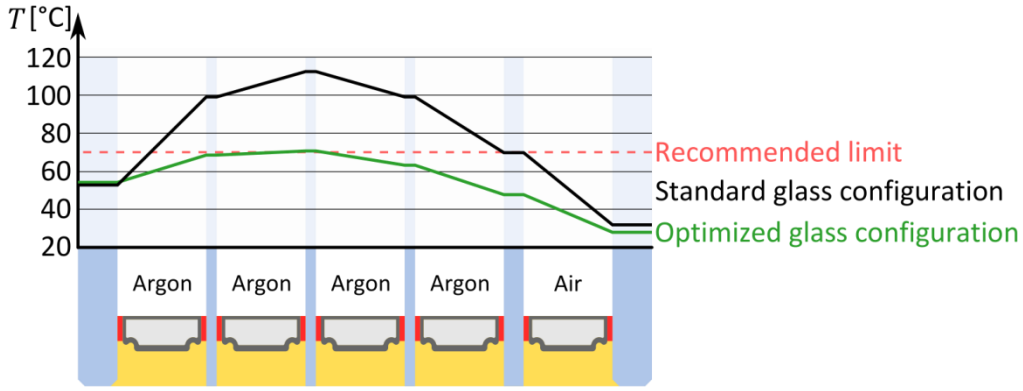

Figure 3. Temperature distribution in the structural elements. The recommended upper limit is the hybrid spacer and PIB primary sealant useful upper temperature limit [10].

3.2. IGU Mechanical Analysis

Thermal loading is the main cause of long-term strains in IGUs with more than three glass panes. The temperature increase in the chambers leads to increased cavity pressure, which affects the gas volume change in the insulation core. The temperature, pressure, and volume in each insulation chamber follow the ideal gas law so as to achieve a static equilibrium. The modelled gas is isothermal, but pressure and volume at equilibrium are affected by the deflection of the glass panes, and the numerical model calculates the equilibrium state. The shape of the unit defines the volume of the given chamber and also recursively affects the pressure within the chamber. It should also be noted that the argon-filled chambers in the investigated six-pane configuration are pneumatically interconnected by 3 mm holes in the intermediate glass panes.

In the FEM model, 20-node quadratic stress/displacement continuum elements are used for the glass panes and sealants, and 8-node doubly-curved thick stress/displacement shell elements are used for the spacers. Additionally, a hydrostatic fluid volume element interconnects the temperature, pressure, and volume of each insulation chamber according to the ideal gas law. The boundary conditions consider an installed IGU as part of a curtain wall facade. A half-model is analysed due to symmetry. The model considers thermal expansion and loading due to cavity pressure. Other load types, e.g., external pressure representing wind loads and glass self-weight, are also considered in the model. The key FEM results needed for further detailed sealant analysis are the displacements of the structural elements attached to the PIB.

3.3. Primary Sealant Mechanical Behaviour

The global FEM model described above gives a general overview of the structural integrity of the product, i.e., the deflection of all panes and their stresses and the strains on the spacers and secondary sealant. It is of major importance for further analysis that this model gives the displacements of all

points of the glass panes and spacers that are in contact with the primary sealant. This provides an opportunity to model the primary sealant separately, where known displacements represent the boundary conditions, as shown in Figure 4.

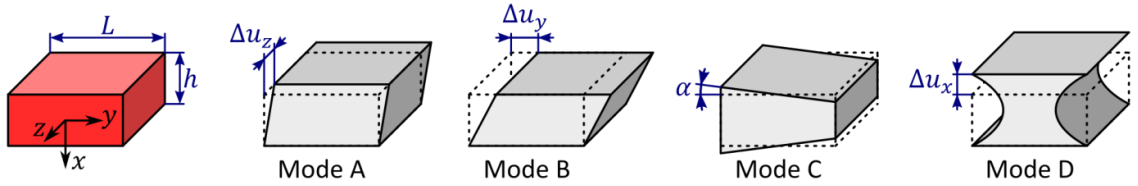

Figure 4. Deformation modes of the primary sealant.

The primary sealant could be analysed as a FEM submodel by prescribing displacements as boundary conditions, but it turns out that such an approach is computationally expensive and has several convergence problems due to the PIB material properties where PIB could be treated as an incompressible solid of very low modulus. For practical reasons, an alternative approach that considers the combined effects of separate deformation modes, with each of them representing a separate task based on the type of loading, was chosen.

Mode A: Shear strains γ_{xz} occur mainly due to the thermal expansion difference between the glass pane and spacer in the longitudinal (z) direction. In cases where a unit is double-symmetric, as presented in Figure 1, γ_{xz} is zero on the symmetry planes and is the highest in the corners. In general, however, self-weight affects shear strains too. We assume that γ_{xz} is location-independent at the PIB cross-section and is dependent on the location on the unit's circumference only; therefore, $\gamma_{xz}(x, y, z) = \gamma_{xz}(z)$ can be calculated from:

$$\gamma_{xz}^{A}(z) = \frac{\Delta u_z(z)}{h} \tag{1}$$

here h is the thickness of the PIB layer.

Mode B: Shear strains γ_{xy} occur due to the thermal expansion difference between the pane and the spacer in the transverse (y) direction and due to the increased cavity pressure in the chamber that loads the spacer from the inner side. Simple shear is assumed for convenience, which means that γ_{xy} is the same over the entire PIB cross-section, hence $\gamma_{xy}(x, y, z) = \gamma_{xy}(z)$. In reality, a spacer made of thin-walled material of low rigidity deforms locally and the spacer wall is no longer precisely parallel with the glass pane; therefore, the average displacements of both contact surfaces with the PIB are needed for the following calculation of the shear strain:

$$\gamma_{xy}^{B}(z) = \frac{\Delta u_y(z)}{h} \tag{2}$$

Mode C: Glass panes bulge under increased cavity pressure; therefore, the glass pane is no longer parallel with the surface of the spacer. The inclination of the PIB layer can be described by the shear strain γ_{xy} and normal strain ε_{xx}. The maximal values of both strains on the PIB cross-section can be approximated with:

$$\varepsilon_{xx}^{C,max}(z) = \pm\frac{L}{h}\tan(\alpha(z)) \tag{3}$$

$$\gamma_{xy}^{C,max}(z) = \pm\alpha(z) \tag{4}$$

Mode D: Increased pressure in the chambers moves the glass panes apart and the role of the secondary sealant is to capture this effect. However, the primary sealant follows the deformations of the secondary sealant, causing the thinning of the primary sealant layer. Obviously, when this deformation mode is established, the PIB layer thins, meaning that the effective cross-section for moisture diffusion increases for the duration of the highest summer climatic loadings and is thus of the highest interest. Moreover, the instantaneously deformed state would not be that critical if the material behaviour of

the primary sealant were not viscoplastic. Low elastic recovery causes a pumping effect during cyclic loading and the loss of sealant integrity; therefore, it is of primary importance that the strain remains as low as possible.

The primary sealant deformation mode D cross-section consists of three strains, ε_{xx}, ε_{yy}, and γ_{xy}. The multiaxial strain state is non-homogeneous and its determination is nontrivial. As will be shown in the results of a case study, mode D is the most influential among all modes, thus the derivation of analytical expressions for all strain components for mode D is crucial and is presented in the next section. The final expression shows that maximal values for the mode D strain field can be expressed as:

$$\varepsilon_{xx}^{D,max}(z) = -\varepsilon_{yy}^{D,max}(z) = 3\frac{\Delta u_x(z)}{h} \tag{5}$$

$$\gamma_{xy}^{D,max}(z) = 2\varepsilon_{xy}^{D,max}(z) = \frac{3L}{h}\frac{\Delta u_x(z)}{h} \tag{6}$$

Total and maximal strain: Once all components of the analysed strain modes are calculated, the same kind of components are combined to get the strain tensor for the multiaxial strain state.

$$\begin{cases} \varepsilon_{xx}(z) = \varepsilon_{xx}^{C,max}(z) + \varepsilon_{xx}^{D,max}(z) \\ \varepsilon_{yy}(z) = \varepsilon_{yy}^{D,max}(z) \\ \gamma_{xy}(z) = \gamma_{xy}^{B}(z) + \gamma_{xy}^{C,max}(z) + \gamma_{xy}^{D,max}(z) \\ \gamma_{xz}(z) = \gamma_{xz}^{A}(z) \end{cases} \tag{7}$$

Strains at different locations are compared via a magnitude of maximal shear strain, calculated as:

$$\gamma_{max}(z) = \sqrt{\left(\varepsilon_{xx}(z) - \varepsilon_{yy}(z)\right)^2 + \gamma_{xy}(z)^2 + \gamma_{xz}(z)^2} \tag{8}$$

4. Derivation of Analytical Expressions for Deformation Mode D

Deformation mode D considers opening or closing the PIB layer between the glass pane and spacer (Figure 5). Relative displacements in the normal direction cause the thinning or thickening of the PIB layer. As shown in Figure 1, the deformation pattern of the PIB cross-section includes normal strains $\varepsilon_{xx}(x,y,z)$, $\varepsilon_{yy}(x,y,z)$, and shear strains $\gamma_{xy}(x,y,z)$. Determination of all these strain field distributions will be based on the following analytical approach.

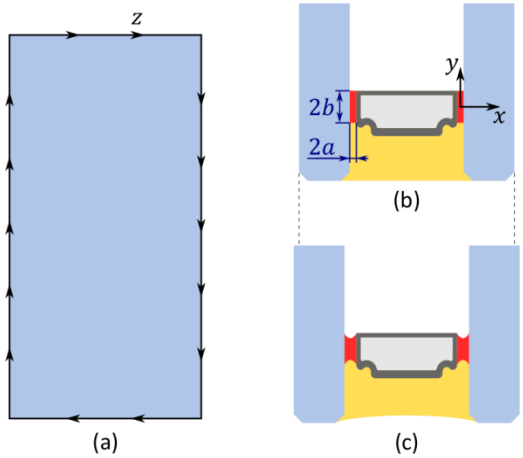

Figure 5. Thinning of the primary sealant layer: (**a**) front view of the unit; (**b**) cross-section before expansion; (**c**) cross-section after expansion.

The first question defines the shape of the PIB when the distance between both surfaces (glass and spacer) increases/decreases. If the PIB is considered to be a liquid medium, the answer is given

by Honschoten et al. [28], who examined the capillary liquid bridge between solid surfaces. Liquid takes a form that minimizes its outer surface area due to surface tension, q_{surf}, which holds a curved differential patch of a doubly-curved liquid surface in equilibrium. Both principal radii of the curvature are related to the Young–Laplace equation, which also considers the pressure difference between the liquid pressure just below the surface and the gas pressure just above the surface, Δp.

$$\frac{1}{R_y} + \frac{1}{R_z} = \frac{\Delta p}{q_{surf}} \tag{9}$$

In the absence of gravitational and electrostatic forces, the pressure gradient inside a fluid is zero. For plane strain conditions, one of the principal radii is infinite, meaning that a cross-sectional curve is a circular arc (Figure 6).

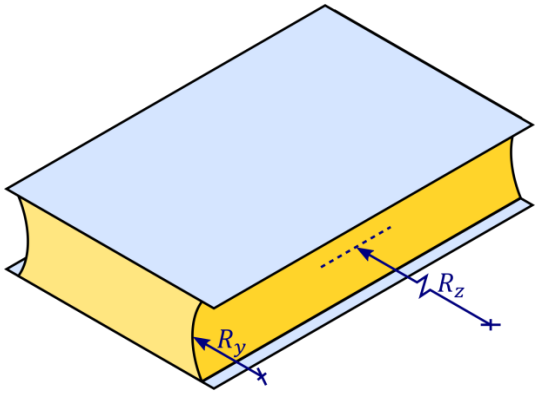

Figure 6. The capillary surface of the plane strain state [28].

For the sake of brevity, let us assume an initially rectangular domain of PIB with dimensions $2a \times 2b$, which is stretched by glass panes in the x-direction. Due to symmetry, only a quarter of the domain is presented in Figure 7. All points of the PIB at $x = a$ are attached on a glass pane, hence their displacements follow the pane, i.e., they move horizontally by Δa. The free surface at $y = b$ forms a circular arc $Y(X, b)$ in a deformed state. We also assume that all points at the same height y also form a circular arc $Y(X, y)$ with radius $R(y)$, which follows the equation:

$$X^2 + (Y(X, y) - B(y))^2 = R(y)^2 \tag{10}$$

where $B(y)$ determines the location of the circle centre for each arc along y and is determined from the condition that each circle must lead through the point $Y(a + \Delta a, y) = y$. Each circular arc is then defined as

$$Y(X, y) = y - \sqrt{R(y)^2 - X^2} + \sqrt{R(y)^2 - (a + \Delta a)^2} \tag{11}$$

where X (location in a deformed state) is assumed to be linearly scaled from the initial domain as:

$$X = X(x) = x\frac{a + \Delta a}{a} \tag{12}$$

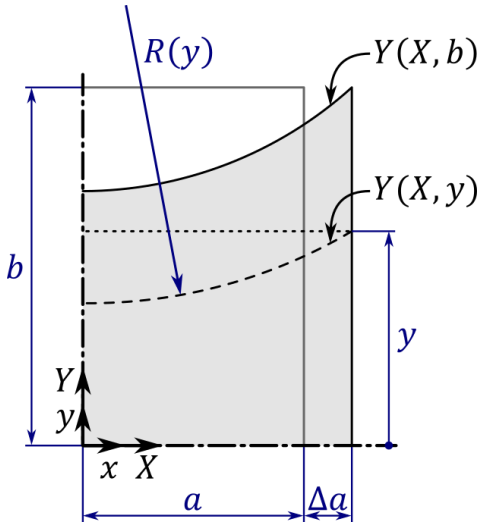

Figure 7. Initial and deformed PIB (a quarter of the domain).

If we consider the incompressibility of the PIB, the radius $R(y)$ is determined from the volume preservation, i.e., the initial volume (or area under plane strain conditions) $V_0(y) = ay$ is the same as the deformed volume (area) $V(y)$, defined as:

$$\begin{cases} V(y) = \int_0^{a+\Delta a} Y(X,y)dX = (a+\Delta a)y + \frac{(a+\Delta a)^2}{2K^2}\left(K\sqrt{1-K^2} - \text{Arcsin}(K)\right) \\ K = K(y) = \frac{a+\Delta a}{R(y)} \end{cases} \tag{13}$$

Considering $V_0(y) = V(y)$, it follows an implicit nonlinear equation for K:

$$y\Delta a + \frac{(a+\Delta a)^2}{2K^2}\left(K\sqrt{1-K^2} - \text{Arcsin}(K)\right) = 0 \tag{14}$$

However, K cannot be extracted explicitly, but since $K \ll 1$, it is admissible to perform a Taylor series expansion for some functions in the above expression. Fourth-order expansions would give $K\sqrt{1-K^2} \approx K - \frac{K^3}{2}$ and $\text{Arcsin}(K) \approx K + \frac{K^3}{6}$, which gives a linear expression for K and consequently it can be extracted as:

$$K = \frac{3y\Delta a}{(a+\Delta a)^2} \tag{15}$$

Which finally gives the linear approximation of the radius $R(y)$:

$$R(y) = \frac{(a+\Delta a)^3}{3y\Delta a} \tag{16}$$

Insertion of $R(y)$ into Equation (11) gives the function of all circular arcs along with the height of domain $Y(X, y)$, which is presented in Figure 7:

$$Y(X,y) = y - \sqrt{\frac{(a+\Delta a)^6}{(3y\Delta a)^2} - X^2} + \sqrt{\frac{(a+\Delta a)^6}{(3y\Delta a)^2} - (a+\Delta a)^2} \tag{17}$$

A point initially located in (x, y) moves to the displaced coordinates (X, Y), hence the vertical displacement is given by $v(x, y) = Y(X(x), y) - y$, which finally gives the vertical component of the displacement field:

$$v(x,y) = \sqrt{\frac{(a+\Delta a)^6}{(3y\Delta a)^2} - (a+\Delta a)^2} - \sqrt{\frac{(a+\Delta a)^6}{(3y\Delta a)^2} - \left(x\frac{a+\Delta a}{a}\right)^2} \tag{18}$$

Considering $\Delta a \ll a$, we can approximate the vertical displacement by means of a Taylor series expansion, which, after rearrangement, gives:

$$v(x,y) = \frac{3y\Delta a}{2a^3}\left(x^2 - a^2\right) \tag{19}$$

Now strains $\varepsilon_{yy}(x, y)$ can be calculated as:

$$\varepsilon_{yy}(x,y) = \frac{\partial v(x,y)}{\partial y} = \frac{3\Delta a}{2a^3}\left(x^2 - a^2\right) \tag{20}$$

The next task is to determine the horizontal displacement component $u(x, y)$. For incompressible solids no volume change occurs, hence, according to small strain theory, the trace of a strain tensor is zero:

$$\varepsilon_{xx}(x,y) + \varepsilon_{yy}(x,y) + \varepsilon_{zz}(x,y) = 0 \tag{21}$$

The elaborated case can be considered as a plane strain problem, where $\varepsilon_{zz}(x, y) = 0$, therefore the absolute values of the strains are the same for the whole domain $\varepsilon_{xx}(x, y) = -\varepsilon_{yy}(x, y)$. Horizontal displacement is now calculated from the definition:

$$u(x,y) = \int -\varepsilon_{yy}(x,y)dx + C(y) \tag{22}$$

Considering the symmetry boundary condition $u(0, y) = 0$, it follows:

$$u(x,y) = \frac{\Delta a}{2}\left(3\frac{x}{a} - \left(\frac{x}{a}\right)^3\right) \tag{23}$$

All displacement and strain fields are presented in Figure 8.

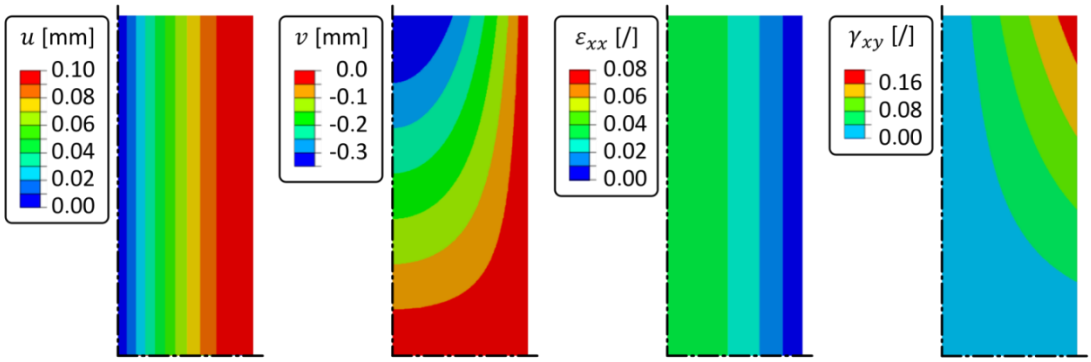

Figure 8. Displacement and strain field without correction.

If the obtained solution is checked with regard to boundary conditions, it is evident that all conditions are fulfilled, except that the shear strains on the free (upper) edge $Y(x, b)$ are not zero, as they should be, since the edge is traction-free. It is reasonable to assume that the solution is a

fair approximation of the far-field strains and displacements, but in the vicinity of the upper edge, the solution has to be upgraded.

For such an upgrade, it is necessary to define the region of influence that the free edge affects. To answer this issue, let us consider the deformation pattern on the free edge. Initially, the regular pattern has to be perpendicular in all free surface points in a deformed state (see Figure 9). The points that are initially at any arbitrary $x = const$ remain a vertical $X = const$ distance from the surface, but tend to incline in the upper region to be perpendicular with the surface. To capture the behavior in the upper part, two functions are defined. The first one is $f_{bound}(x)$, which divides both regions, and the second one is $f_{corr}(y)$, which will help to define the correction of the horizontal displacement field in the upper part, i.e., $y \geq f_{bound}(x)$. It turns out that both functions can be defined as quadratic functions, $f_{bound}(x) = a_1 + a_2 x + a_3 x^2$ and $f_{corr}(y) = a_4 + a_5 y + a_6 y^2$ (see Figure 9).

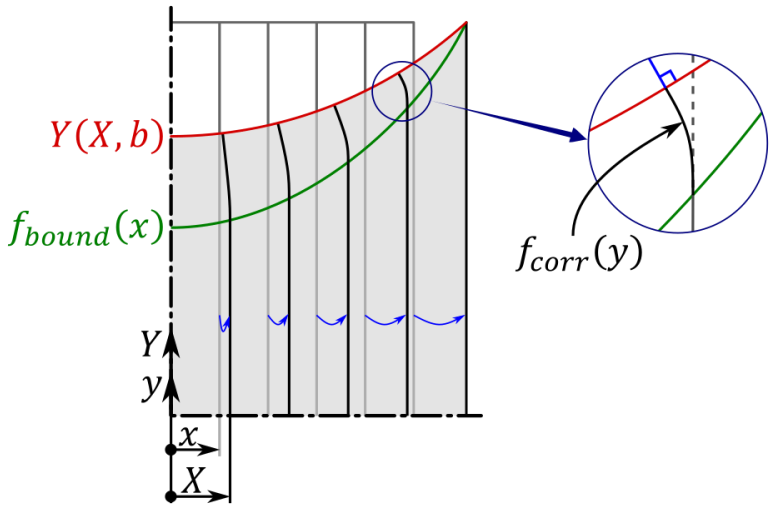

Figure 9. Correction of the displacement field.

There are six parameters for both functions, which are defined according to the following assumptions:

- $f_{corr}(f_{bound}(x)) = 0$: The function f_{corr} will not correct the far-field solution of the horizontal displacement of points lying on the boundary.
- $f'_{corr}(b) = -\frac{\partial}{\partial x} Y(x, b)$: The perpendicularity of the parabola f_{corr} and circular arc $Y(x, b)$ on the surface.
- $f'_{corr}(f_{bound}(x)) = 0$: The smooth transition of the deformed curve, which was initially $x = const$ between both regions.
- $f_{bound}(a) = b$: The points that are close to the right edge cannot have a wide region of correction. Although on the surface the condition of perpendicularity must be fulfilled, below the surface the points have to reach a vertical position not far from the surface; the limit case is exactly the right edge, which is vertical by definition, hence the correction from the inclined upper surface to the vertical position has to be theoretically made at a single point, i.e., in the upper right corner.
- $f'_{corr}(0) = 0$: Assuming the symmetry of the influential region is reasonable.
- $f_{bound}(0) = b - a_7$: This equation defines the range of the function f_{bound} on the symmetry plane, but according to the new unknown a_7, another condition is needed. The free surface far from the right edge is traction-free (and consequently has no strains) on the free surface, hence let us consider $\varepsilon_{xx}(0, b) = 0$. However, the strains must take into consideration the new displacement field, which already includes the correction:

$$\varepsilon_{xx}(0, b) = \frac{\partial}{\partial x}(u(x, b) + f_{corr}(b))\Big|_{x=0} = 0 \tag{24}$$

The equation system is linear and all seven unknowns, a_1 to a_7, can be obtained analytically. Using known functions, the upgraded displacement field can be defined as:

$$u_{ALL}(x,y) = u(x,y) + \begin{cases} f_{corr}(y) & ; \quad y > f_{bound}(x) \\ 0 & ; \quad y \le f_{bound}(x) \end{cases} \tag{25}$$

Once $u_{ALL}(x,y)$ is known, $v_{ALL}(x,y)$ is derived analogically to Equation (22). Without the loss of generality, the solution can be converted into a more convenient form using non-dimensional variables $\xi = \frac{x}{a}$, $\eta = \frac{y}{b}$ and $\varepsilon_0 = \frac{\Delta a}{a}$. The final solution of the displacement field is:

$$\begin{cases} u_{ALL}(\xi,\eta) = \frac{a\xi\varepsilon_0(3-\xi^2)}{2} - \begin{cases} u_{corr}(\xi,\eta) & ; \quad \eta > f_{bound}(\xi) \\ 0 & ; \quad \eta \le f_{bound}(\xi) \end{cases} \\ u_{corr}(\xi,\eta) = \frac{3\xi\varepsilon_0\left(a^2(1-\xi^2)-b^2(1-\eta)\right)^2}{2a^3(1-\xi^2)} \end{cases} \tag{26}$$

$$\begin{cases} v_{ALL}(\xi,\eta) = -\frac{3b\varepsilon_0\eta(1-\xi^2)}{2} - \begin{cases} v_{corr}(\xi,\eta) & ; \quad \eta > f_{bound}(\xi) \\ 0 & ; \quad \eta \le f_{bound}(\xi) \end{cases} \\ v_{corr}(\xi,\eta) = \frac{\varepsilon_0\left(a^2(1-\xi^2)-b^2(1-\eta)\right)^2\left(a^2(1-6\xi^2+5\xi^2)-b^2(1+\xi^2)(1-\eta)\right)}{2a^4b(1-\xi^2)^2} \end{cases} \tag{27}$$

where $f_{bound}(\xi) = 1 - \left(\frac{a}{b}\right)^2\left(1-\xi^2\right)$. The displacement and strain fields are presented in Figure 10 for $a = 4$mm, $b = 10$mm, and $\Delta a = 0.1$mm.

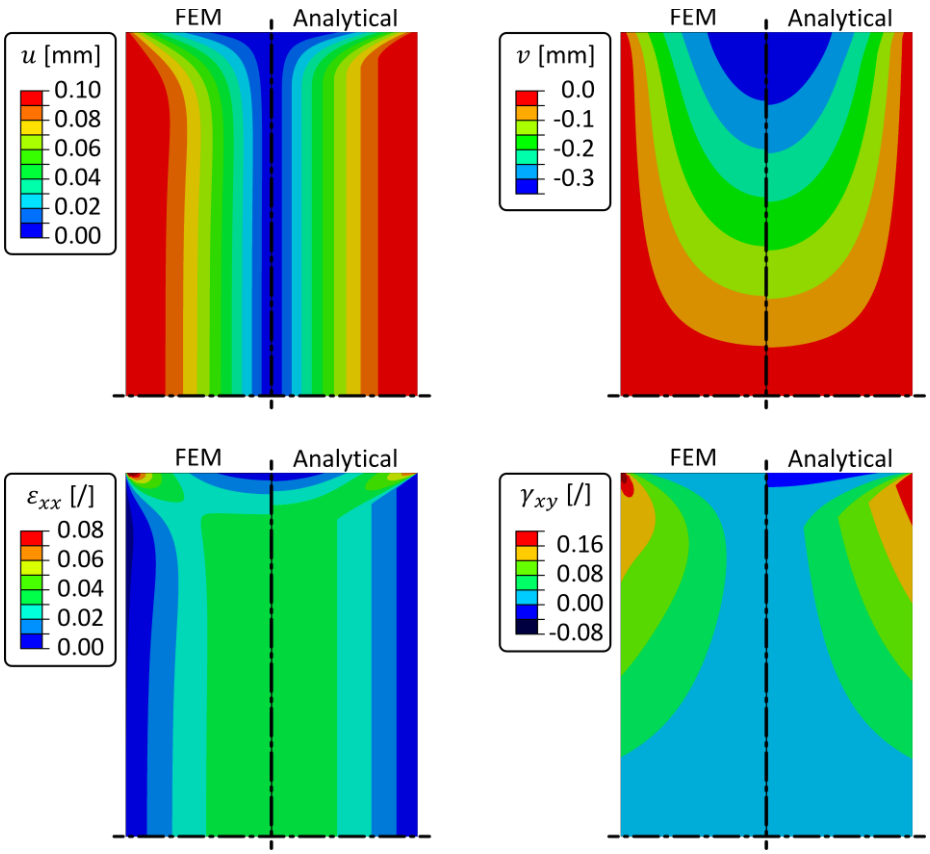

Figure 10. Displacement and strain fields; left half: finite element method (FEM) results, right half: analytical results.

As a final result, we can also extract extreme values for all strains. Extreme values are in the rightmost and uppermost corner, i.e., in the location ($\xi = \eta = 1$):

$$\varepsilon_{xx}^{max} = -\varepsilon_{yy}^{max} = 3\varepsilon_0 \tag{28}$$

$$\varepsilon_{xy}^{max} = \frac{3b}{2a}\varepsilon_0 \tag{29}$$

Verification: In the presented derivation, there are a moderate number of assumptions and approximations. The first check of the final solution correctness is to verify the fulfilment of the boundary conditions. The displacement field Equations (26) and (27) give $u_{ALL}(0, \eta) = 0, v_{ALL}(\xi, 0) = 0$ and $u_{ALL}(1, \eta) = a\varepsilon_0 = \Delta a$, which confirms that all kinematic boundary conditions are exactly met.

The second verification is related to the entire displacement and strain fields. Analytical expressions will be compared with the results of a numerical analysis performed with the finite element method using the Abaqus FEM program [29].

In FEM, a domain 4 mm × 10 mm has been discretized into 4000 plane strain 8-node biquadratic hybrid elements (Abaqus notation CPE8H). The left and lower edges have been symmetrically supported, and on the right edge vertical displacements have been restrained, while the horizontal displacements are defined as Δa =0.1 mm. The upper edge is traction free. The results are presented in Figure 10 and a comparison with the analytical displacement and strain field confirms that the derived expressions, which have a quite manageable form, are a fair approximation of the strain field calculations of the presented problem.

5. Results and Discussion

5.1. Reference Case

The described methodology gives the strain state in all layers of the primary sealant in a multipane IGU, but there exist no standardised allowable values to compare this strain state with. In order to obtain allowable values, we will rely on engineering practice. SIKA Facade Systems [30] are well known for their long use in civil engineering, which proves the longevity of such units. From a mechanical point of view, the behaviour of SIKA double glass units (DGUs) can be analysed by means of the same methodology as described above, and such a calculation will be called a reference case.

The calculated primary sealant strains in this reference case are conservatively treated as the maximal strains that the primary sealant is capable of withstanding, which represents the allowable strain value for the primary sealant of any other arbitrary IGU configuration. It is reasonable to assume that a new IGU configuration is feasible if its primary sealant strains do not exceed the values from the reference case.

For this reason, we chose a classic 1 m high and 0.5 m wide double glass unit 6-12-6 at 20 kPa internal overpressure for analysis using the same methodology. Figure 11 presents the maximal shear strain on the primary sealant along the edge of both layers for one-quarter of the model. The strains are equal in both layers due to the symmetrical unit configuration 6-12-6 and the presence of thermal loads only. The analysis reveals that the pressure change in mode D has by far the greatest impact on the total strain. The maximal shear strain distribution has two extreme values, the first in the middle of the longest edge due to the expansion of the glass panes, and the second in the corner due to the compression of the deformed, i.e., doubly-curved, glass panes.

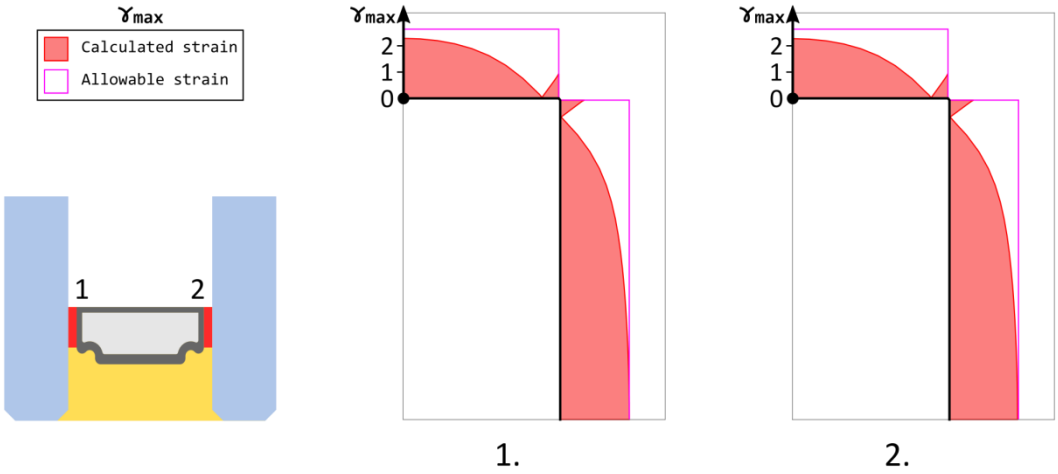

Figure 11. Maximal shear strain on both PIB layers 1-2 along the circumference of the reference unit.

The analysis of the reference DGU conservatively considers only climatic loading and no other external loads, e.g., self-weight, wind loads, etc. In this specific case, the absolute maximal value is reached in the middle of the longest edge. Since the longevity of the DGU is verified through engineering practice, the values from Figure 11 will be called the reference values and the maximum will be used as the allowable strain in the feasibility assessment of a newly designed multipane IGU.

In the next subsection, the multipane IGU strain will be compared with the allowable strain. If the calculated primary sealant strain in all locations of the IGU is below the allowable strain, the longevity of the analysed IGU is confirmed.

5.2. Analysis of the Multipane IGU

The same methodology as for the DGU is also used for the above-described six-pane IGU. The analysis considers climate loading, self-weight, and wind load. Wind load is modelled as a uniform pressure of 3.6 kPa, which is equivalent to a wind gust of about 250 km/h.

The six-pane IGU has 10 layers of primary sealant. The maximal shear strain distribution for all the layers is presented in Figure 12. The analysis is performed in three consecutive steps: in the first one only self-weight is considered, in the second step thermal loading is added, and finally, wind load is applied.

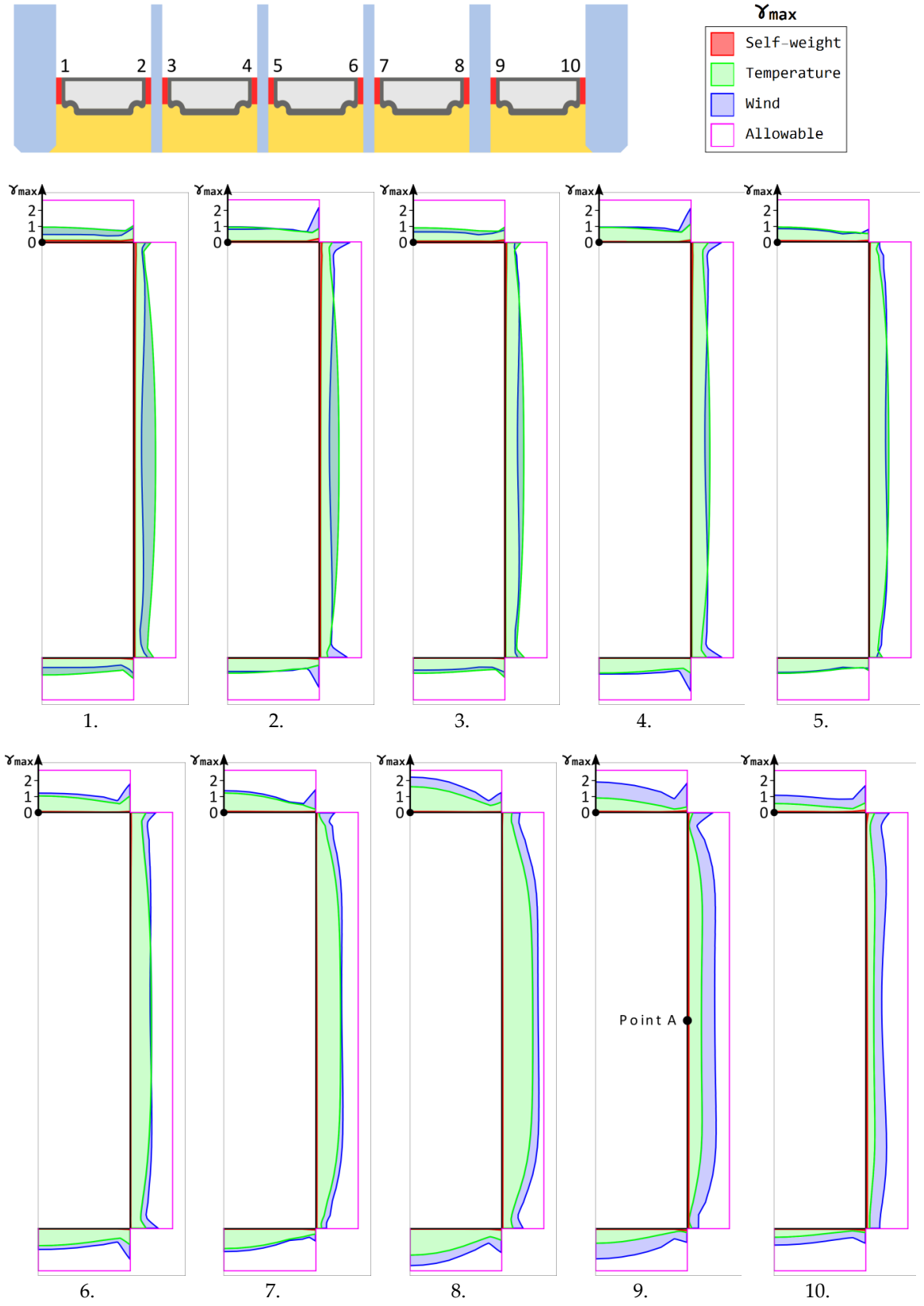

Figure 12. Maximal shear strain distribution in each layer 1-10 of the primary sealant along the edge of the six-pane Q-Air glazing unit.

The results reveal that shear strains caused by self-weight are classified as mode A on the vertical edges and mode B on the horizontal edges and are significantly lower in comparison to the other loadings. In the final step, the thermal loads are applied, which cause all four modes, but it is evident that mode D is by far the most dominant deformation mode due to its large contribution to the magnitude of the strain components (Figure 13). The same observation is recorded for the wind load, which means that the transverse pressure loading caused either by chamber temperature increase or wind loads has a much more important effect on the primary sealant strains than shear strains due to the self-weight or glass temperature difference.

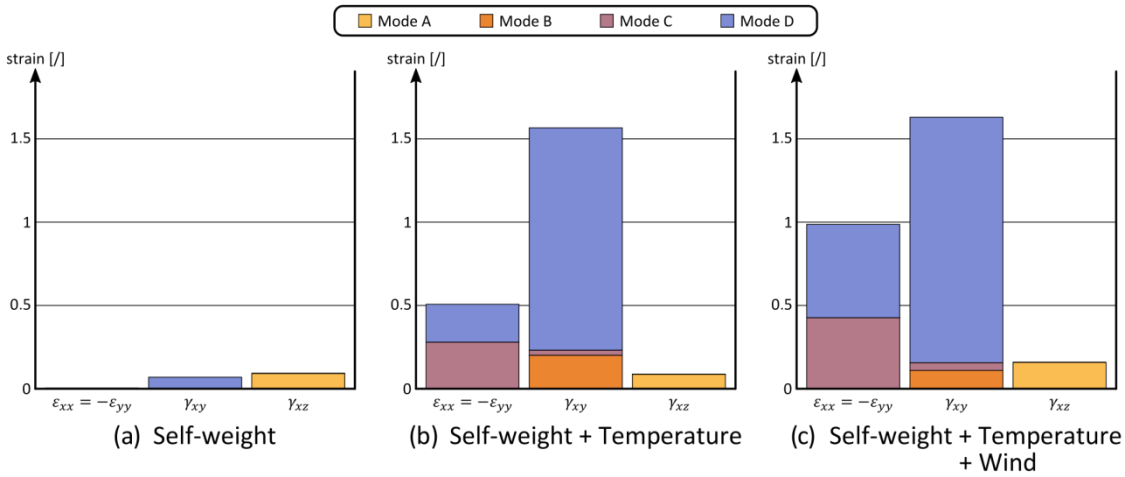

Figure 13. The contribution of deformation modes to the strain components in the primary sealant for different load cases (**a**) self-weight, (**b**) self-weight + temperature, (**c**) self-weight + temperature + wind; location on the edge: Point A (cf. Figure 12).

The most important result of this analysis is that the maximal strains are below the allowable strain. The maximal shear strains in the six-pane Q-Air glazing unit also take into consideration self-weight and wind loads, but they are still below the allowable strain, which was calculated using climatic loading of 20 kPa internal over-pressure, as described in the previous section. It can be also noticed that the strains in the middle of the edge and in the corner are in the same range and that there is no especially highly loaded region, which can become critical during the lifetime of the unit. From these results, the value of such an analysis for the design phase can be recognised. The described methodology can provide answers to the composition of a multipane IGU where strains in all primary sealant layers are sufficiently low.

5.3. Practical Aspects

Quadruple glazing is a cost-efficient solution. Quadruple glazing offers glazing with U_w values as low as 0.4 W/m^{2}K, which is sufficient to abandon otherwise common external, modulated sun-shading and trading for the solar control coating. Abandoning of external sun-shading is sufficient to offset for the cost of the extra glass pane whose add-on cost is at about 10€/m^2, so payback is immediate as savings are direct on the up-front basis when compared with triple-pane glazing with external sun-shading. Cost benefits don't end here. In some cases, it is possible to abandon central heating for the building and make the building so-called "zero heating". A further advantage is marked acceptance. In Norway, for example, there are many triple glazed buildings now in their third or fourth decade—ready to be refurbished.

Four to six-pane Q-Air units were first produced in 2010 and have subsequently been field-tested since 2012. Industrial property for handling sealed chamber insulating gas pressure variations and for handling temperature effects for intermediate panes and sealants was obtained. Their first commercial application was in 2014. Six-pane Q-Air glazing units were used in a major renovation of

the Wergelandsveien 7 building in Oslo (Figure 14), where the old triple-pane glazing with thermal transmittance of glass U_g-value 2.2 W/(m^{2}K) was replaced with the new system with a U_g-value of 0.24 W/(m^{2}K). A total of 550 small fixed glass, window-size, six-pane units were installed in 2015. In 2016 a further 20 large (jumbo) size six-pane units were installed on the ground floor. The presented methodology has been used for durability assessment in a design phase of the Q-Air.

Figure 14. The Wergelandsveien 7 building in Oslo before (**left**) and after renovation (**right**) [10].

6. Conclusions

Primary sealant strain is of great significance to insulating glass unit (IGU) lifetime. After cyclic loading with excessive strain, the seal functionality of the insulation chambers can be prematurely compromised. Excessive thinning of the primary sealant increases moisture permeation and may provoke premature fogging of the glass panes.

The presented new methodology assesses the strain state in all primary sealant layers. The strain state is based on the displacement of the surrounding structural elements, determined by a global FEM model. Primary sealant strains are then calculated using derived analytical expressions. The methodology considers the combination of four deformation modes arising from different loading scenarios. The most influential and of the highest interest is the extension of the sealant (i.e., mode D), which is also the most challenging to characterize due to its multiaxial strain state. Such behaviour cannot be described with simple engineering expressions. The main theoretical contribution of the paper is thus a derivation of analytical expressions for a strain field estimation for deformation mode D, which is the most influential among all the other modes.

The analyses reveal that an increase in pressure in the insulating chambers following a temperature increase represents by far the most significant influence on the sealant strain state; therefore, pressure variations in the insulating chambers should be a major concern in the design phase of any multipane IGU. This means that self-weight and differences in linear thermal expansion coefficients play only a minor role in multipane IGU durability.

Our method is built on the assumption of proportional loading from the initial state. However, during the lifetime of any IGU very complex loading occurs, i.e., cyclic weather conditions (summer/winter), stochastic external loads (wind), etc. Since the behaviour of incompressible primary sealant can be described as perfectly plastic, loading history plays a crucial role. It would seem impossible to determine realistic sealant strains during an unknown loading history, thus the presented methodology is based on a comparison of the maximal strain in two glass units, where the first one is an already established reference maximum from civil engineering practice and the second is the

newly designed unit. If the peak strain in the investigated unit does not exceed the allowable strain, it is deemed that the unit is validated and ready to be applied in practice. The developed methodology thus represents a useful tool for IGU durability assessment.

Author Contributions: Conceptualization, B.S. and M.H.; methodology, A.M. and M.H.; software, P.R. and Š.O.; validation, A.K.; formal analysis, B.S., A.M. and M.H.; investigation, B.S., A.M., P.R., M.H.; resources, A.K.; data curation, A.K. and P.R.; writing—original draft preparation, B.S., P.R. and M.H.; writing—review and editing, B.S. and M.H.; visualization, A.M.; supervision, M.H.; project administration, P.R., M.H.; funding acquisition, M.H. All authors have read and agreed to the published version of the manuscript.

Funding: This research was funded by the Slovenian Research Agency (grant number P2-0263).

Acknowledgments: The authors acknowledge the financial support received from the Slovenian Research Agency (research core funding No. P2-0263).

Conflicts of Interest: The authors declare no conflicts of interest.

References

1. Stetson, T.D. Improvement in Window Glass. U.S. Patent 49167, 1 August 1865.
2. Van Den Bergh, S.; Hart, R.; Jelle, B.P.; Gustavsen, A. Window spacers and edge seals in insulating glass units: A state-of-the-art review and future perspectives. *Energy Build.* **2013**, *58*, 263–280. [CrossRef]
3. Carbary, L.D.; Kimberlain, J.H. Structural silicone glazing: Optimizing future designs based on historical performances. *Intell. Build. Int.* **2018**, 1–11. [CrossRef]
4. Klosowski, J.; Wolf, A.T. *Sealants in Construction*, 2nd ed.; CRC Press: Boca Raton, FL, USA, 2016.
5. Torok, G.R. Predicting Time-to-Fogging of Insulating Glass Units. In Proceedings of the 11th Canadian Conference on Building Science and Technology, Banff, Alberta, 21–23 March 2007.
6. Garvin, S.L.; Wilson, J. Environmental conditions in window frames with double-glazing units. *Constr. Build. Mater.* **1998**, *12*, 289–302. [CrossRef]
7. Burgess, J.C. The history, scientific basis and application of international IGU durability tests. *Build. Environ.* **1999**, *34*, 363–368. [CrossRef]
8. Knorr, M.D.; Wieser, J.; Geertz, G.; Buddenberg, S.; Oechsner, M.; Wittwer, W. Gas loss of insulating glass units under load: Internal pressure controlled permeation test. *Glass Struct. Eng.* **2016**, *1*, 289–299. [CrossRef]
9. Domjan, S.; Arkar, C.; Begelj, Z.; Medved, S. Evolution of all-glass nearly Zero Energy Buildings with respect to the local climate and free-cooling techniques. *Build. Environ.* **2019**, *160*, 106183. [CrossRef]
10. Kralj, A.; Drev, M.; Znidarsic, M.; Cerne, B.; Hafner, J.; Jelle, B.P. Investigations of 6-pane glazing: Properties and possibilities. *Energy Build.* **2019**, *190*, 61–68. [CrossRef]
11. Wolf, A.T. Silicone Sealed Insulating Glass Units. In Proceedings of the ISAAG—International Symposium on the Application of Architectural Glass-Engineering and Architectural Design of Glass, Munich, Germany, 15–16 November 2004.
12. Wolf, A.T.; Waters, L.J. Factors governing the life expectancy of dual-sealed insulating glass units. *Constr. Build. Mater.* **1993**, *7*, 101–107. [CrossRef]
13. Foraboschi, P. Analytical modeling to predict thermal shock failure and maximum temperature gradients of a glass panel. *Mater. Des.* **2017**, *134*, 301–319. [CrossRef]
14. Scherer, C.; Semar, E.; Wittwer, W.; Wolthaus, J.; Scherer, T. A New Reactive Thermoplastic Spacer with Excellent Durable Energy Efficiency for Structural Glazing Façades. *Chall. Glass Conf. Proc.* **2016**, *5*, 233–248. [CrossRef]
15. Asphaug, S.K.; Jelle, B.P.; Gullbrekken, L.; Uvslokk, S. Accelerated ageing and durability of double-glazed sealed insulating window panes and impact on heating demand in buildings. *Energy Build.* **2016**, *116*, 395–402. [CrossRef]
16. IGMA-GANA. *TB-1250-XX, Polyisobutylene (PIB) Primary Sealant*; Insulating Glass Manufacturers Alliance, Glass Association of North America: Ottawa, ON, Canada, 2017.
17. Wolf, A. New development in the field of insulating glass units. *Constr. Build. Mater.* **1988**, *2*, 134–144. [CrossRef]
18. Wolf, A.T. Studies into the Life-Expectancy of Insulating Glass Units. *Build. Environ.* **1992**, *27*, 305–319. [CrossRef]

19. Ihara, T.; Gustavsen, A.; Jelle, B.P. Sealant aging and its correlation with facade reflectance. *Constr. Build. Mater.* **2014**, *69*, 390–402. [CrossRef]
20. Song, S.Y.; Jo, J.H.; Yeo, M.S.; Kim, Y.D.; Song, K.D. Evaluation of inside surface condensation in double glazing window system with insulation spacer: A case study of residential complex. *Build. Environ.* **2007**, *42*, 940–950. [CrossRef]
21. Park, S.; Song, S.Y. Thermally improved triple-glazing windows considering the condensation resistance (TDR) and thermal transmittance (U-factor) to meet Korean standards. *Build. Simul. China* **2019**, *12*, 87–98. [CrossRef]
22. Wolf, A.T. *Design and Material Selection Factors That Influence the Service-Life and Utility Value of Dual-Sealed Insulating Glass Units*; Dow Corning SA: Barcelona, Spain, 2002.
23. Grynning, S.; Jelle, B.P.; Gustavsen, A.; Gao, T.; Time, B. Multilayer glazing technologies: Key performance and future perspectives. In Proceedings of the CLIMA 2016—12th REHVA World Congress, Aalborg, Denmark, 22–25 May 2016; Volume 2.
24. Hagl, A. Experimental and Numerical Analysis of Edge Seal Spacers of Insulated Glass Units for Structural Sealant Glazing Applications. In *Challenging Glass 3*; Delft University Press: Delft, The Netherlands, 2012; pp. 221–234. [CrossRef]
25. Stewart, J.; Brien, W.; Wolf, A. Quantification of Differential Thermal Movement in Insulating Glass Edge Seals Using Finite Element Analysis. *J. Astm Int.* **2006**, *3*, 1–7. [CrossRef]
26. Rosendahl, P.L.; Staudt, Y.; Schneider, A.P.; Schneider, J.; Becker, W. Nonlinear elastic finite fracture mechanics: Modeling mixed-mode crack nucleation in structural glazing silicone sealants. *Mater. Des.* **2019**, *182*, 108057. [CrossRef]
27. Window. *Window 7.4 Manual, Lawrence Berkeley National Laboratory*; Window: Berkeley, CA, USA, 2016.
28. van Honschoten, J.W.; Tas, N.R.; Elwenspoek, M. The profile of a capillary liquid bridge between solid surfaces. *Am. J. Phys.* **2010**, *78*, 277–286. [CrossRef]
29. Abaqus. Abaqus 6.12 Documentation, Dassault Systemes. 2012. Available online: http://130.149.89.49:2080/v6.12/index.html (accessed on 19 February 2020).
30. SIKA. *SIKA Facade Systems: Sealing and Bonding in Facades—Specification Guide*; Innovation and Consistency: Zurich, Switzerland, 2016.